Journal of Materials Chemistry A

One-pot synthesis of microporous carbons highly enriched in nitrogen and their electrochemical performance

Journal:	*Journal of Materials Chemistry A*
Manuscript ID:	TA-ART-06-2014-002959.R1
Article Type:	Paper
Date Submitted by the Author:	30-Jun-2014
Complete List of Authors:	Fuertes, Antonio B; Instituto Nacional del Carbon (CSIC), Ferrero, Guillermo A.; Instituto Nacional del Carbon (CSIC), Sevilla, Marta; Instituto Nacional del Carbon, Quimica de Materiales

One-pot synthesis of microporous carbons highly enriched in nitrogen and their electrochemical performance

A. B. Fuertes, G. A. Ferrero and M. Sevilla*

Instituto Nacional del Carbón (CSIC), P.O. Box 73, Oviedo 33080, Spain

* Corresponding author: martasev@incar.csic.es; Fax: +34 985 297662; Tel: +34 985 119090.

Abstract

Microporous carbons with large nitrogen contents (6 - 23 wt%) have been successfully synthesized by the co-carbonization of an alkali organic salt and melamine. In this way, the processes of carbonization, activation and incorporation of nitrogen heteroatoms into the carbon backbone are integrated in only one step. The general applicability of this simple procedure has been proved by using it with a variety of organic salts, including potassium gluconate, and sodium salts of gluconate, citrate and alginate. In particular, the materials produced from potassium gluconate have a narrow micropore size distribution centered at around 0.7 - 0.8 nm, BET surface areas up to 1040 $m^2 \cdot g^{-1}$, and pore volumes of ~ 0.3 - 0.4 $cm^3 \cdot g^{-1}$. It was found that the presence of abundant N-groups enhances the electrochemical performance of these materials in 1 M H_2SO_4. They exhibit high specific capacitances (surface basis), in the 16.6 – 23 $\mu F \cdot cm^{-2}$ range and a good electro-oxidation stability as evidenced by the fact that carbon oxidation is shifted to more positive potentials by as much as 500 mV with respect to undoped carbon. In particular, a supercapacitor built with the carbon material synthesized at 850 ºC using a melamine/potassium gluconate weight ratio of 2 showed an excellent robustness over a voltage window of 1.2 V in 1 M H_2SO_4, providing a maximum energy density of 10.2 $Wh \cdot kg^{-1}$ (7.9 $Wh \cdot L^{-1}$) and maximum power density of 5.7 $kW \cdot kg^{-1}$ (4.4 $kW \cdot L^{-1}$).

1. Introduction

The incorporation of nitrogen into the framework of carbon materials has recently generated a great deal of interest in relation to their use in electrochemical applications such as metal-free ORR (oxygen reduction reaction) catalysts, [1] supercapacitor electrodes [2] and Li-ion battery anodes. [3] Indeed, it has been reported that N-doped porous carbons clearly exhibit a superior performance as supercapacitors due to an enhancement of their electronic conductivity[4] and surface wettability[5] in addition to the pseudo-capacitive effects contributed by the nitrogen functional groups.[6] Several synthetic strategies are commonly used to introduce nitrogen heteroatoms into the structure of porous carbons: a) thermal post-treatment by employing reactive nitrogen-containing reagents (*i.e.* NH_3, urea, cyanamide, etc) [7-9], b) the use as carbon precursors of N-doped polymers obtained by polycondensation of certain organic monomers including nitrogen-rich compounds (*i.e.* pyrrole, aniline, urea, melamine, hydroxypyridine, acrylonitrile, etc) [10-14] and c) the carbonization of materials with high nitrogen contents such as ionic liquids [15] or biomass-derived products.[16-18] The first method involves complex and time-consuming steps. In addition, the doped carbon has a low nitrogen content and the N-groups are mostly inserted in the surface instead of the bulk of the material. By contrast, the other two methods are simpler since the use of a nitrogen-rich compound leads directly to carbons with N-groups uniformly distributed throughout the material. However, the nitrogen content of the N-carbons produced in this way decreases dramatically with a rise in temperature. As an example, the porous carbons produced by chemical activation of polypyrrole at 800 ºC have nitrogen contents lower than 1 %. [19] Thus, a simple and sustainable method of preparing carbon materials with a well-developed porosity and large nitrogen contents has still to be found.

We recently developed a straightforward one-step template-free method for the production of porous carbons based on the use of alkali organic salts as precursors.[20] These organic salts combine a carbon precursor (*i.e.* the organic moiety) and alkali elements (*i.e.* Na or K) that are able to generate during heat-treatment inorganic species capable of operating as activating agents. In the present work, we have gone further and, on the basis of our previous

methodology, we have developed a facile and efficient one-step strategy to produce high-content, nitrogen-doped, microporous carbons. The procedure involves the co-carbonization of a mixture formed by an organic salt and melamine. That allows the processes of carbonization, activation and incorporation of nitrogen heteroatoms into the carbon backbone to be performed in only one step. Additionally, we demonstrate the positive effect of N-doping on the enhancement of the specific capacitance through pseudocapacitance phenomena and the improvement of electro-oxidation stability. In this way, it was possible to operate a supercapacitor over a voltage window of 1.2 V in 1 M H_2SO_4, storing 10 W h kg^{-1} at 0.03 kW kg^{-1} and 5 W h kg^{-1} at 3 kW kg^{-1} (drain time = 6s) with an excellent long-term stability.

2. Experimental

2.1. Materials

Potassium gluconate, sodium gluconate, sodium citrate, sodium alginate and melamine were obtained from Aldrich and used without further purification.

2.2. Synthesis of Materials

1 g of potassium gluconate and 2 g or 4 g of melamine were grounded to form a homogeneous mixture, which was then heat-treated under nitrogen in a quartz reactor up to the desired temperature at a heating rate of 3 ºC·min^{-1} and maintained at this temperature for 1 hour. Subsequently, the black solid residue was washed with diluted HCl (10 wt%). Finally, the carbon sample was collected by filtration, washed with abundant distilled water and dried at 120 ºC for several hours. The materials thus synthesized were denoted as *CN- x - y*, where *x* is the temperature (in ° C) and *y* the (melamine/organic salt) weight ratio. For comparison purposes, a carbon was produced by simple carbonization of potassium gluconate at 800 ºC. This sample was denoted as *C-KG*.

2.3. Characterization

The nitrogen sorption isotherms of the carbon samples were measured at −196 °C using a Micromeritics ASAP 2020 sorptometer. The apparent surface area

(S_{BET}) was calculated from the N_2 isotherms using the BET method. An appropriate relative pressure range was selected to ensure that a positive line intersect of multipoint BET fitting (C > 0) would be obtained and that the $V_{ads}(1 - p/p_o)$ value would increase with p/p_o.[21, 22] The total pore volume (V_p) was determined from the amount of nitrogen adsorbed at a relative pressure (p/p_o) of 0.95. The micropore volume (V_m) was obtained by applying a t-plot analysis (Harkins and Jura thickness equation) to the N_2 sorption isotherms. [23] The micropore size distributions were determined by applying the Quenched-Solid Density Functional Theory (QSDFT) method to the nitrogen adsorption data and assuming a slit-pore model. Scanning electron microscopy (SEM) images were obtained on a Quanta FEG650 (FEI) instrument. Transmission electron micrographs (TEM) were taken on a JEOL (JEM 2100-F) apparatus operating at 200 kV. X-ray diffraction (XRD) patterns were obtained on a Siemens D5000 instrument operating at 40 kV and 20 mA, using CuKa radiation. X-ray photoelectron spectroscopy (XPS) was carried out on a Specs spectrometer, using Mg Kα (1253.6 eV) radiation from a double anode at 150 W. Binding energies for the high resolution spectra were calibrated by setting C 1s to 284.6 eV. Elemental analysis (C, N and O) of the samples was carried out on a LECO CHN-932 microanalyzer. The Raman spectra were recorded on a Horiva (LabRam HR-800) spectrometer. The source of radiation was a laser operating at a wavelength of 514 nm and at a power of 25 mW. Thermogravimetric analysis (TGA) curves were recorded on a TA Instruments Q600 TGA system.

The dc electrical conductivity of the carbon powders was determined on a home-made apparatus (four-probe method) by pressing the powders between two plungers into a hollow Nylon cylinder (inner diameter of 8 mm), and applying a pressure of 7.1 MPa. This apparatus allowed the simultaneous determination of conductivity and packing density.

2.4. Electrochemical measurements

Electrodes were prepared from a paste composed of 85 wt% of active material, 10 wt% of polytetrafluoroethylene (PTFE) binder (Aldrich, 60 wt% suspension in water) and 5% Super P (Timcal). The electrochemical measurements were performed in two- and three-electrode Swagelok™ type cells fitted with

stainless steel current collectors. The electrochemical characterization was carried out using a computer-controlled potentiostat (Biologic VMP3 multichannel generator).

The two-electrode cells were constructed using two carbon electrodes of comparable mass and thickness (loading of active material: ~6-7 $mg \cdot cm^{-2}$, diameter of pellets: 1 cm), electrically isolated by a glassy fibrous separator. A 1 M H_2SO_4 solution was used as electrolyte. Cyclic voltammetry (CV) was conducted in the voltage range of 0 to 0.8-1.2 V at 2 $mV \cdot s^{-1}$. Galvanostatic charge/discharge cycling (CD) was performed in the same voltage range at increasing current densities over the 0.05 – 10 $A \cdot g^{-1}$ range (on the basis of the active mass of a single electrode). The values of gravimetric capacitance or surface area-normalized capacitance (with respect to the BET surface area) provided throughout the text correspond to a single electrode.

To trace the Ragone plots, the specific energy ($Wh \cdot kg^{-1}$) was calculated by means of the following formula:

$$E = \frac{1}{2} C_{cell} \Delta V_d^{\ 2} \qquad (4)$$

where C_{cell} is the gravimetric capacitance of the total cell ($F \cdot g^{-1}$) and ΔV_d is the operation voltage (V_{max} – IR drop).

The specific power ($kW \cdot kg^{-1}$) was calculated by means of the formula:

$$P = \frac{E}{\Delta t_d} \qquad (5)$$

where Δt_d is the discharge time.

As previously mentioned, three-electrode measurements were also performed, using a graphite rod as counter electrode, Hg/Hg_2SO_4 as the reference electrode (SME) and 1 M H_2SO_4 as the electrolyte. Cyclic voltammetry experiments were performed at 2 $mV \cdot s^{-1}$ over different varying potential working windows.

3. Results and discussion

3.1. Formation of N-doped porous carbons

When melamine is heat-treated in an open system, it completely sublimates at a temperature of ~ 330 ºC as can be seen from in Figure S1 in the Supporting Information (SI). However, the sublimation can be suppressed to a large extent if the melamine is heat-treated together with other substances with a capacity to bridge the melamine molecules.[24] This occurred in the present work. When the melamine was heated up to ~ 500 ºC in the presence of an organic salt, a large fraction of the melamine did not sublimate but polymerized to give a carbon nitride allotrope (*g*-C_3N_4). As a result, the treatment of a mixture of organic salt/melamine at 500 ºC gave rise to a material formed by a carbonaceous matter and *g*-C_3N_4. The presence of carbon nitride in this sample was clearly demonstrated by the XRD measurements. As can be seen from Figure 1a, the XRD pattern of the CN-500-4 sample exhibits two peaks at ~14º and 27.4º, which are typical of *g*-C_3N_4. [25] The strongest peak at 27.4º can be attributed to the (*002*) reflection characteristic of graphite-like stacking of *g*-C_3N_4 sheets. When the carbonization temperature increases from 500 ºC to 800 ºC, two processes occur in parallel: i) the carbonization of the organic salt and ii) the decomposition of carbon nitride, which completely decomposes at < 750 ºC. [26] In this way, N-doped carbons are produced due to the reaction between the semi-carbonized organic salt and the reactive nitrogen-containing species (*e.g.* $C_2N_2^+$, $C_3N_2^+$, $C_3N_3^+$, etc) generated during the decomposition of carbon nitride. [24, 27, 28] The carbonization and decomposition processes were monitored by means of thermogravimetric analysis (TGA). Figure 1b shows a comparison of the weight loss curves corresponding to potassium gluconate and a sample synthesized at 500 ºC (*i.e.* CN-500-4). The TGA curve for potassium gluconate displays two weight losses at 200-450 ºC and at ~ 800 ºC, which can be ascribed respectively to the pyrolysis of the organic moiety and the activation/gasification process of the carbonaceous matter. [20] By contrast, the TGA curve corresponding to the CN-500-4 sample exhibits a large weight loss that starts at ~ 550 ºC and finishes at around 700 ºC. This weight loss is assigned to the decomposition of carbon nitride, the percentage of this compound being around 75 wt %. The small weight loss observed at T > 750 ºC

is attributed to the activation processes associated with the carbonaceous residue derived from potassium gluconate (*vide supra*). The above results show that the carbon nitride is completely decomposed at 700 ºC and that the incorporation of nitrogen in the carbon backbone is likely to occur within this temperature range (*i.e.* 550-700 ºC). These findings suggest that the N atoms of the samples prepared at ≥ 800 ºC belong to the doped carbon rather than to any residual compound.

3.2. Structural characteristics of the carbon materials

The crystalline structure of the samples obtained at temperatures in the 500-900 ºC range was investigated by carrying out XRD measurements (Figure 1a). The materials obtained at low temperatures (*i.e.* CN-500-4 and CN-650-4) show a weak band at ~14º and an intense peak at 27.4º (d_{002}=0.325 nm), which is assigned to carbon nitride g-C_3N_4 (*vide supra*). At higher carbonization temperatures, the band at ~14º completely disappears while the (*002*) peak shifts to lower angles, indicating an increase in stacking distances towards values typical of turbostratic carbons (*i.e.* d_{002}=0.336 nm at 800 ºC, d_{002}=0.345 nm at 850 ºC and d_{002}=0.357 nm at 900 ºC). Interestingly, the N-carbon exhibits a certain graphitic order which is clearly superior to that of the undoped carbon (C-KG). This suggests that the graphite-like stacking of *g*-C_3N_4 is preserved to some extent in the structure of the N-carbons.

The morphology and structure of the N-carbons were first examined by scanning electron microscopy (SEM) and transmission electron microscopy (TEM). Figure 2 gathers representative SEM and TEM images obtained for the CN-850-4 sample. Figure 2a shows that the N-carbon particles have a sponge-like structure formed by fully interconnected thin layers (see Figure 2b) unlike the carbon produced by simple carbonization of potassium gluconate which consists of vesiculated compact particles (see Figure S2 in SI). The porosity of these N-carbons is made up of randomly distributed uniform micropores, as illustrated by the high-resolution transmission electron microscopy images in Figures 2c and 2d. This observation is consistent with the textural properties deduced from the analysis of the N_2 sorption isotherms. Figure 3 displays the nitrogen sorption isotherms and micropore size distributions for the two series of samples prepared using melamine/organic salt weight ratios of 2 and 4 at three

different temperatures (*i.e.* 800 ºC, 850 ºC and 900 ºC). It can be seen that all the samples exhibit a type I isotherm, which is typical of microporous materials (Figure 3a). Moreover, these isotherms have narrow knees at low relative pressures, indicating narrow pore size distributions. This is confirmed by the micropore size distributions in Figure 3b, which show that the micropores are very narrow, ~ 0.7-0.8 nm. The textural properties deduced from an analysis of the nitrogen isotherms are listed in Table 1. Whereas the samples synthesised at lower temperatures (*i.e.* 500 ºC and 650 ºC) are essentially non-porous (S_{BET} < 5 $m^2 \cdot g^{-1}$), the N-carbons produced at ≥ 800 ºC possess high BET surface areas ranging from 660 to 1040 $m^2 \cdot g^{-1}$ and pore volumes of ~ 0.3-0.4 $cm^3 \cdot g^{-1}$ corresponding almost exclusively to micropores (< 2 nm). In comparison with the undoped carbon, the N-doped samples show a poorer textural development. Thus, while the CN-800-4 carbon is a microporous material with a BET surface area of 660 $m^2 \cdot g^{-1}$ and a pore volume of 0.29 $cm^3 \cdot g^{-1}$, the undoped C-KG sample has a porosity made up of micropores and mesopores, with a BET surface area of 1410 $m^2 \cdot g^{-1}$ and a pore volume of 0.76 $cm^3 \cdot g^{-1}$. [20] This result together with the information deduced from a comparison of the particle morphologies (SEM images) and the XRD patterns corresponding to the N-doped and undoped carbons (*vide supra*) show that the processes of formation and decomposition of *g*-C_3N_4 not only determine the chemical properties of the N-carbons but also their structural characteristics.

3.3. Chemical properties of N-doped carbons

The chemical compositions of the synthesized materials determined by elemental analysis are listed in Table 1. It can be seen that the percentage of nitrogen decreases substantially with the rise in temperature from 47.8 wt % in the case of CN-500-4 to 6.3 wt % for the CN-900-4 sample. A similar variation can be observed in the samples obtained with a melamine/organic salt ratio of 2. In connection with this, the (N/C) atomic ratio undergoes a sharp reduction with temperature (see Figure S3 in SI). These changes are to be expected given that at high temperatures nitrogen is thermodynamically more stable in a molecular form. [29] The energy-dispersive X-ray (EDX) analysis of a CN-800-4 particle yields an (N/C) atomic ratio of 0.31 (Figure S4b) which is in close agreement with the value determined by elemental analysis (0.33). The

distribution of C and N was analyzed from elemental mapping images of several CN-800-4 particles (see Figures S4c and S4d in SI). Both the EDX analysis and the C and N mappings indicate that nitrogen is uniformly distributed throughout the N-carbon particles.

The elemental analysis gives the amounts of nitrogen and carbon but does not provide any information about the chemical environments of these elements or about the modification they undergo with temperature. This information is crucial for verifying the chemical nature of the synthesized materials. Therefore, XPS measurements were performed on samples synthesized at 500 ºC and 800 ºC (Figure 4). As can be seen, the deconvoluted high-resolution N 1s XPS spectrum for the CN-500-4 sample (Fig. 4a) exhibits two peaks that can be assigned to C-N=C (398.4 eV) and N-$(C)_3$ (400.4 eV) groups. These peaks are characteristic of carbon nitride (*g*-C_3N_4),[24, 30] confirming that the material obtained at 500 ºC is a mixture of carbonaceous matter and carbon nitride. This is corroborated by the C 1s XPS spectrum corresponding to the CN-500-4 sample (Fig. 4b). Here there are two main peaks that are ascribed to aromatic or other sp^2-hybridised carbon atoms bound to neighboring carbon atoms or hydrogen (284.6 eV, ~ 36 %) [31] and C-N=C groups (287.9 eV). [24, 32] An additional less pronounced deconvoluted peak at 285.9 eV is assigned to C-O bonding configurations (~ 10 %). The peak at 287.9 eV is clearly associated to carbon nitride, while the peaks at 284.6 eV and 285.9 eV can be ascribed to the carbonaceous matter resulting from the carbonization of potassium gluconate. In the case of the material obtained at 800 ºC (CN-800-4), the deconvolution of the N 1s spectrum reveals three peaks corresponding to N-pyridinic (398.1 eV, 51 %) and N-pyrrolic/N-pyridonic (400.1 eV, 44 %), and a minor contribution at 401.9 eV (5 %) ascribed to N-quaternary (Fig. 5a). [33] These nitrogen functional groups are characteristic of carbons that contain N-heteroatoms incorporated into the graphene layers. On the other hand, the C 1s spectrum for the CN-800-4 sample is typical of porous carbons, with a main peak at 284.6 eV (~ 50 %) corresponding to sp^2 C-C bonds and other less-intense peaks (*i.e*. 285.8 eV, 288.3 eV and 290.1 eV) associated to oxygen/nitrogen groups (Fig. 4b). These results prove that the materials synthesized at temperatures ≥ 800 ºC are N-doped carbons containing nitrogen

functional groups within the carbon backbone. Furthermore, a comparison of the N/C atomic ratio derived from the elemental analysis (0.33, Table 1) and the N/C ratio obtained by XPS (0.19) suggests that almost half of the nitrogen species are in the surface and therefore readily accessible to act as catalytic sites, participate in redox reactions, etc.

For the above experiments we employed potassium gluconate, but N-doped carbons with similar properties can also be obtained by using other organic salts. To confirm this, we used sodium salts of gluconate, citrate and alginate. In these experiments, mixtures of organic salt/melamine were heat-treated at 800 ºC for one hour. As in the case of the CN-800-4 sample, such N-carbons have very high nitrogen contents and BET surface areas of ~ 600 $m^2 \cdot g^{-1}$, with a porosity made up exclusively of narrow micropores of around 1 nm in size. The structural properties and chemical compositions of these N-carbons are summarized in the Supporting Information (for details see Table S1 and Figures S5, S6 and S7). At this point, it is worthwhile drawing attention to the exceptional properties of the N-carbons synthesised at temperatures ≥ 800 ºC, *i.e.* extremely high nitrogen contents (*e.g.* 22.9 wt % for CN-800-4) and a well-developed microporosity.

3.4. Electrochemical properties

As mentioned in the Introduction, the nitrogen doping of carbon materials is well known for its beneficial effects. These include an improved electronic conductivity (due to the additional electrons introduced by nitrogen atoms within the aromatic structure), an enhanced thermal/oxidation stability and catalytic activity in electron transfer reactions (ORR), a better wettability and pseudocapacitance. Some of these beneficial effects have been observed in the present study when analyzing the supercapacitor performance in 1 M H_2SO_4 solutions of the CN-800-2, CN-850-2 and CN-900-2 materials, in particular the improvements related to wettability, oxidation stability and pseudocapacitance.

The electronic conductivity of the carbon samples was measured using a four-probe method. It was found that, whereas the undoped carbon (C-KG) exhibits a high electronic conductivity (3.7 $S \cdot cm^{-1}$), the N-carbons have conductivities of 2.5, 0.4 and 0.03 $S \cdot cm^{-1}$ for CN-900-2, CN-850-2 and CN-800-

2, respectively. It can be seen, therefore, that the conductivity decreases with an increase in the N content. This is due to the fact that the N groups mainly correspond to pyridinic and pyrrolic moieties (95 % according to XPS measurements), which do not provide electrons to the delocalized π-system, unlike the N-quaternary groups. Besides, larger N contents are accompanied by a higher number of defect sites which might disrupt the π-system. [34] This is supported by the Raman spectra in Figure S8 (SI) which show that the intensity of the D band (related to imperfections in sp^2 carbon structures) is higher than that of the G band in CN-800-2 (associated to the E_{2g2} vibrational mode of sp^2 bonded carbon atoms in graphene sheets), whereas the opposite is the case for C-KG and CN-900-2, indicating the introduction of a large number of defect sites with increased N-doping.

The study of the pseudocapacitance and electrochemical oxidation stability of the N-carbons was carried out using a three-electrode configuration. The three-electrode CV curves obtained are shown in Figure 5a. In this graph, capacitance is expressed as surface area-normalized capacitance (termed S-capacitance), which allows a better visualization of the pseudocapacitance contributions. For comparison purposes, the curve for the undoped carbon (C-KG) has also been included. It can be seen that the S-capacitance correlates directly with the nitrogen content, as illustrated in Figure 5c. What is more, the S-capacitance of the N-doped carbons is noticeably superior to that of the undoped carbon C-KG, which clearly suggests a pseudocapacitance contribution due to the presence of N-groups. Furthermore, an improved wettability was observed after N-doping, which might have increased the double-layer capacitance. On the other hand, the results in Figure 5a reveal that the voltage working window may be enlarged as the nitrogen content increases. Thus, the voltage window extends from 0.9 V for the undoped sample C-KG to 1.1 V for CN-900-2, 1.3 V for CN-850-2 and 1.35 V CN-800-2. It should be noted that the thermodynamic potential limits for water reduction (H_2 formation) and oxidation (O_2 formation), in 1 M H_2SO_4, are – 0.62 V (*vs.* SME) and 0.56 V (*vs.* SME) respectively. Significantly, the enlargement of the voltage window is caused not only by the increase in the overpotential for water reduction but, more importantly, because carbon oxidation is shifted to more positive

potentials, closer to the thermodynamic value for water oxidation. This finding is very important for the potential use of these N-carbons in oxidative environments such as the anodic compartment of a fuel cell and it has been previously observed in relation to oxygen-rich carbons.[35] It should be noted that, whereas the CV curve for C-KG (9.4 wt % O) shows a well-located hump at around -0.1 - 0 V *vs.* SME, which is ascribable to redox reactions involving the quinone/hydroquinone pair or pyrone-like structures, [35-37] the CV curves obtained for the N-carbons exhibit a broad hump over the whole range of negative potentials up to ~0.2 V *vs.* SME, which can be attributed to the multiple redox reactions involving N-groups. Thus, in addition to the faradaic reactions involving the oxygen moieties, the pyrrolic/pyridonic and pyridinic groups present in the N-carbons are involved in several faradaic processes as illustrated in Scheme 1.

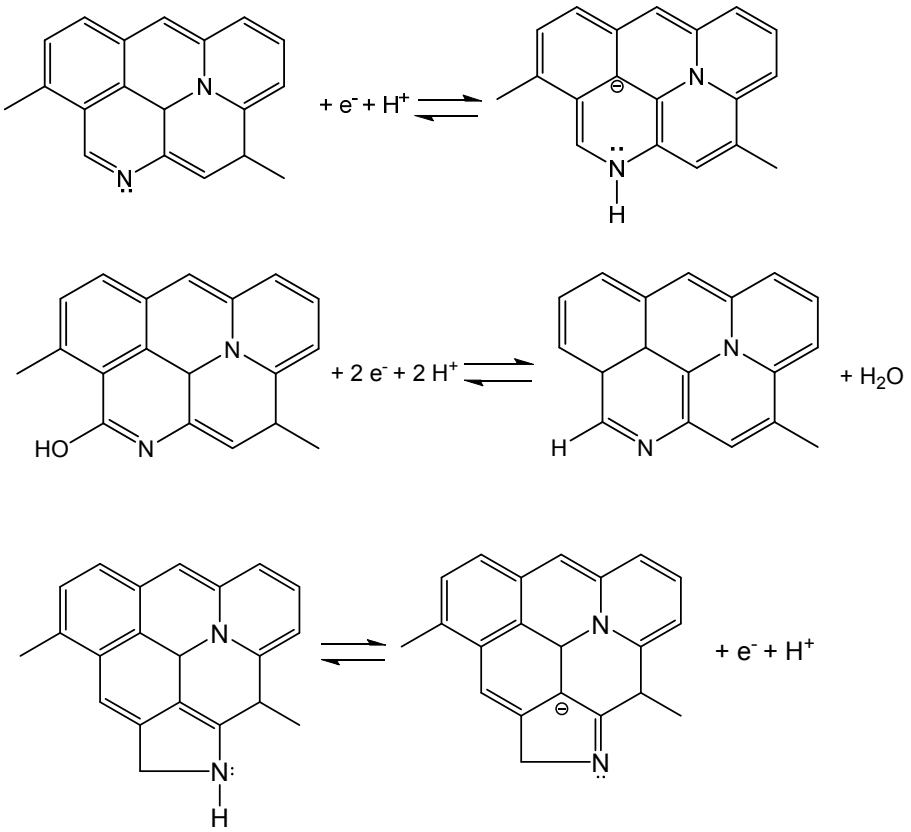

Scheme 1. Possible faradaic charge transfer reactions involving: (1) pyridinic, (2) pyridonic and (3) pyrrolic nitrogen groups. [38]

The real supercapacitor performance of the carbon samples was obtained using a two-electrode system. It can be observed from the CV curves obtained from this configuration (Figure 5b) that the values of S-normalized capacitance are lower than those obtained with a three-electrode configuration. This suggests that the faradaic reactions are not being fully exploited in the working voltage range of the two-electrode symmetrical supercapacitor. Further improvement of capacitance could therefore be achieved either through mass balancing in an asymmetrical supercapacitor or by increasing the voltage window in a symmetrical supercapacitor. As observed in the three-electrode system, the S-capacitance values deduced from the experiments performed using a two-electrode configuration (Figure 5b) steadily increase with the nitrogen content (Figure 5c). S-capacitance values in the ~ 19 – 50 $\mu F \cdot cm^{-2}$ range have been previously reported in the literature for other N-doped porous carbons (N content < 15 %) with a two-electrode cell and H_2SO_4 electrolyte. [39-42] The data represented in Figure 5c reveal that the incorporation of nitrogen produces a marked increase in specific capacitance, by as much as 72 % for CN-800-2 (~ 17 wt % N) compared to the undoped C-KG sample.

In order to determine the gravimetric capacitance accurately, galvanostatic charge-discharge (CD) experiments were performed at current densities of up to 10 $A \cdot g^{-1}$. The results disclosed in Figure 6a show that the N-doped carbons possess values of specific capacitance in the 170 – 190 $F \cdot g^{-1}$ range at 0.1 $A \cdot g^{-1}$, which registers a 20 – 40 % decrease with the increase in current density up to 10 $A \cdot g^{-1}$. For C-KG, the loss in capacitance at 10 $A \cdot g^{-1}$ is 23 %. The larger fading of capacitance for the N-carbons is probably a consequence of their lower conductivity, as well as the slower kinetics of the redox reactions compared to the formation of the double-layer. Interestingly, the N-carbons exhibit high packing densities, increasing from 0. 71 $g \cdot cm^{-3}$ for CN-900-2 to 1.1 $g \cdot cm^{-3}$ for CN-800-2, which are higher than that of C-KG (0.51 $g \cdot cm^{-3}$). This result is worth noting as it means that these samples will exhibit high volumetric capacitances, as illustrated in Figure 6b. What is especially remarkable is that these volumetric capacitances are higher than those recorded in aqueous electrolytes for carbide-derived carbons (both powders

and monoliths), [43-45] and many activated carbons [46-50] and mesoporous carbons [51-55] with larger gravimetric capacitances.

To assess the energy and power characteristics, we selected the CN-850-2 sample owing to its high specific capacitance (186 $F \cdot g^{-1}$ at 0.1 $A \cdot g^{-1}$), good rate capability and large voltage stability window (up to ~ 1.3 V). Taking into account this last feature, we investigated the electrochemical behavior of this carbon as the cell voltage varied from 0.8 V to 1.2 V (Figure 7). The cyclic voltammetry curves in Figure 7a, which exhibit the characteristic rectangular shape, reveal that neither decomposition of the electrolyte nor carbon corrosion takes place even at low scan rates (2 $mV \cdot s^{-1}$). This conclusion is confirmed by the galvanostatic charge/discharge experiments carried out at a low discharge rate of 0.1 $A \cdot g^{-1}$, which show the typical symmetric features with a coulombic efficiency of ≥ 95 % (Figure 7b). These results indicate that this N-carbon is stable over a wide voltage window up to 1.2 V, which agrees with the three-electrode measurements (see Figure 5a). Besides, when the cell voltage is increased from 0.8 V to 1 V and 1.2 V, the current increases both in the cathodic and anodic scans (Figure 7a), which can be ascribed to redox reactions involving N-groups, as illustrated in the three-electrode tests. Thus, pseudocapacitance is being exploited more fully and the specific capacitance of the two-electrode cell is closed to that of the three-electrode cell. To examine the stability of the supercapacitor over these voltage windows, charge/discharge cycling experiments were performed at 5 $A \cdot g^{-1}$ for 6000 cycles successively at 0.8, 1.0 and 1.2 V, and then for 5000 additional cycles at 10 $A \cdot g^{-1}$ and 1.2 V (Figure 8a). Capacitance loss at a discharge current of 5 $A \cdot g^{-1}$ was as low as 4 % at 0.8 V, and 2 % at 1.0 and 1.2 V, while at 10 $A \cdot g^{-1}$ and 1.2 V, the loss of capacitance was negligible. This N-carbon sample therefore exhibits excellent stability even at 1.2 V in 1 M H_2SO_4. The increase in specific capacitance and especially the widening of the working voltage window (as $E = ½ C V^2$) translated into an enhancement of the energy stored from 4.2 $Wh \cdot kg^{-1}$ (3.2 $Wh \cdot L^{-1}$) at 0.8 V to 10.2 $Wh \cdot kg^{-1}$ (7.9 $Wh \cdot L^{-1}$) at 1.2 V. This can be clearly visualized in the Ragone plot displayed in Figure 8b. A maximum energy density of 10.2 $Wh \cdot kg^{-1}$ (7.9 $Wh \cdot L^{-1}$) and maximum power density of 5.7 $kW \cdot kg^{-1}$ (4.4 $kW \cdot L^{-1}$) were achieved. This value of specific energy is comparable, or

close, to that achieved in organic electrolyte (2 V) with some mesoporous carbons [56] and commercial activated carbons such as Norit Supra 50 (see Figure 8b). Moreover, this increase in the amount of energy stored is not at the expense of specific power as occurs with organic electrolytes, where the ionic conductivity is lower.

4. Conclusions

In summary, we have described a one-step strategy for fabricating microporous carbons with high nitrogen contents, in the 6 - 23 wt% range. This material is produced by the co-carbonization of an alkali organic salt and melamine, and by integrating the carbonization, activation and incorporation of nitrogen heteroatoms into the carbon backbone in only one step. The presence of abundant N-groups in these microporous carbons greatly enhances their electrochemical performance in 1 M H_2SO_4. It was found that these N-carbons exhibit high specific capacitances (surface basis), in the 16.6 – 23 $\mu F \cdot cm^{-2}$ range, and a good electro-oxidation stability, as evidenced by the fact that carbon oxidation is shifted to more positive potentials by as much as 50 up to 500 mV with respect to the undoped carbon. The CN-850-2-based supercapacitor was able to operate in a voltage window of 1.2 V in 1 M H_2SO_4, storing 10 $Wh \cdot kg^{-1}$ at 0.03 $kW \cdot kg^{-1}$ and 5 $Wh \cdot kg^{-1}$ at 3 $kW \cdot kg^{-1}$ (drain time = 6s) with an excellent long-term stability.

Acknowledgments. This research work was supported by Spanish MINECO (MAT2012-31651). G. A. F. thanks the Ministerio de Economía y Competitividad of Spain for his predoctoral contract and M. S. thanks the Ministerio de Ciencia e Innovación of Spain for her Ramón y Cajal contract.

References

1. Y. Zheng, Y. Jiao, M. Jaroniec, Y. Jin and S. Z. Qiao, *Small*, 2012, **8**, 3550-3566.
2. E. Frackowiak, Q. Abbas and F. Béguin, *Journal of Energy Chemistry*, 2013, **22**, 226-240.
3. Y. Mao, H. Duan, B. Xu, L. Zhang, Y. Hu, C. Zhao, Z. Wang, L. Chen and Y. Yang, *Energy Environ. Sci.*, 2012, **5**, 7950-7955.
4. D. Hulicova, M. Kodama and H. Hatori, *Chemistry of Materials*, 2006, **18**, 2318-2326.
5. W. Shen and W. Fan, *J. Mater. Chem. A*, 2013, **1**, 999-1013.

6. K. Fic, E. Frackowiak and F. Beguin, *J. Mater. Chem.*, 2012, **22**, 24213-24223.
7. D.-W. Wang, F. Li, L.-C. Yin, X. Lu, Z.-G. Chen, I. R. Gentle, G. Q. Lu and H.-M. Cheng, *Chemistry – A European Journal*, 2012, **18**, 5345-5351.
8. J. P. Boudou, M. Chehimi, E. Broniek, T. Siemieniewska and J. Bimer, *Carbon*, 2003, **41**, 1999-2007.
9. K. Parvez, S. Yang, Y. Hernandez, A. Winter, A. Turchanin, X. Feng and K. Müllen, *ACS Nano*, 2012, **6**, 9541-9550.
10. D. Hulicova, J. Yamashita, Y. Soneda, H. Hatori and M. Kodama, *Chemistry of Materials*, 2005, **17**, 1241-1247.
11. A. B. Fuertes and T. A. Centeno, *J. Mater. Chem.*, 2005, **15**, 1079-1083.
12. A. Lu, A. Kiefer, W. Schmidt and F. Schüth, *Chemistry of Materials*, 2004, **16**, 100-103.
13. M Perez-Cadenas, C. Moreno-Castilla, F. Carrasco-Marin and A. F. Perez-Cadenas, *Langmuir* 2009**, 25***,* 466-470.
14. J. Patiño, M. C. Gutierrez,a D. Carriazo, C. O. Ania, J. L. G. Fierro, M. L. Ferrera and F. del Monte, *J. Mater. Chem. A*, 2014, **2**, 8719–8729.
15. T.-P. Fellinger, A. Thomas, J. Yuan and M. Antonietti, *Adv. Mater.*, 2013, **25**, 5838-5855.
16. L. Zhao, N. Baccile, S. Gross, Y. Zhang, W. Wei, Y. Sun, M. Antonietti and M. M. Titirici, *Carbon*, 2010, **48**, 3778-3787.
17. H. Sun, W. He, C. Zong and L. Lu, *ACS Appl. Mater. Interfaces* 2013, **5**, 2261−2268.
18. X. Y. Chen, C. Chen, Z. J. Zhang and D. H. Xie, *J. Mater. Chem. A*, 2013, **1**, 10903–10911.
19. M. Sevilla, P. Valle-Vigon and A. B. Fuertes, *Adv. Funct. Mater.*, 2011, **21**, 2781-2787.
20. M. Sevilla and A. B. Fuertes, *J. Mater. Chem. A*, 2013, **1**, 13738-13741.
21. F. Rouquerol, J. Rouquerol and K. Sing, *Adsorption by powders and porous solids: principles, methodology and applications*, Academic Press, San Diego 1999.
22. *ISO 9277:2010. Determination of the specific surface area of solids by gas adsorption - BET method. Second Edition of ISO 9277, ISO*; Geneva, 2012.
23. S. J. Gregg and K. S. W. Sing, *Adsorption, surface area and porosity*, Academic Press, London [etc.], 1991.
24. A. Thomas, A. Fischer, F. Goettmann, M. Antonietti, J.-O. Muller, R. Schlogl and J. M. Carlsson, *J. Mater. Chem.*, 2008, **18**, 4893-4908.
25. M. Groenewolt and M. Antonietti, *Adv. Mater.*, 2005, **17**, 1789-1792.
26. Y. C. Zhao, D. L. Yu, H. W. Zhou, Y. J. Tian and O. Yanagisawa, *Journal of materials science*, 2005, **40**, 2645-2647.
27. Z. Wen, X. Wang, S. Mao, Z. Bo, H. Kim, S. Cui, G. Lu, X. Feng and J. Chen, *Adv. Mater.*, 2012, **24**, 5610-5616.
28. Z.-H. Sheng, L. Shao, J.-J. Chen, W.-J. Bao, F.-B. Wang and X.-H. Xia, *ACS Nano*, 2011, **5**, 4350-4358.
29. K. K. R. Datta, V. V. Balasubramanian, K. Ariga, T. Mori and A. Vinu, *Chemistry – A European Journal*, 2011, **17**, 3390-3397.
30. Q. Guo, Y. Xie, X. Wang, S. Zhang, T. Hou and S. Lv, *Chem. Commun.*, 2004, 26-27.
31. J. F. Moulder and J. Chastain, *Handbook of X-ray Photoelectron Spectroscopy: A Reference Book of Standard Spectra for Identification and Interpretation of XPS Data*, Physical Electronics Division, Perkin-Elmer Corporation, 1992.
32. V. N. Khabashesku, J. L. Zimmerman and J. L. Margrave, *Chemistry of Materials*, 2000, **12**, 3264-3270.
33. J. R. Pels, F. Kapteijn, J. A. Moulijn, Q. Zhu and K. M. Thomas, *Carbon*, 1995, **33**, 1641-1653.
34. N. Daems, X. Sheng, I. F. J. Vankelecom and P. P. Pescarmona, *J. Mater. Chem. A*, 2014, **2**, 4085-4110.
35. E. Raymundo-Piñero, M. Cadek and F. Béguin, *Adv. Funct. Mater.*, 2009, **19**, 1032-1039.
36. V. Ruiz, C. Blanco, E. Raymundo-Piñero, V. Khomenko, F. Béguin and R. Santamaría, *Electrochim. Acta*, 2007, **52**, 4969-4973.

37. C. T. Hsieh and H. Teng, *Carbon*, 2002, **40**, 667-674.
38. F. Béguin, E. Raymundo-Piñero and E. Frackowiak, in *Carbons for Electrochemical Energy Storage and Conversion Systems*, CRC Press, 2010, pp. 329-375.
39. M. Seredych, D. Hulicova-Jurcakova, G. Q. Lu and T. J. Bandosz, *Carbon*, 2008, **46**, 1475-1488.
40. D. Hulicova-Jurcakova, M. Seredych, G. Q. Lu and T. J. Bandosz, *Adv. Funct. Mater.*, 2009, **19**, 438-447.
41. E. J. Ra, E. Raymundo-Piñero, Y. H. Lee and F. Béguin, *Carbon*, 2009, **47**, 2984-2992.
42. X. Yang, D. Wu, X. Chen and R. Fu, *The Journal of Physical Chemistry C*, 2010, **114**, 8581-8586.
43. J. Chmiola, G. Yushin, R. Dash and Y. Gogotsi, *J. Power Sources*, 2006, **158**, 765-772.
44. J. Chmiola, Y. Gogotsi, C. Largeot and P. Simon, *Meeting Abstracts*, 2008, **MA2008-02**, 419.
45. J. A. Fernández, M. Arulepp, J. Leis, F. Stoeckli and T. A. Centeno, *Electrochim. Acta*, 2008, **53**, 7111-7116.
46. K. Torchała, K. Kierzek and J. Machnikowski, *Electrochim. Acta*, 2012, **86**, 260-267.
47. G. Hasegawa, M. Aoki, K. Kanamori, K. Nakanishi, T. Hanada and K. Tadanaga, *J. Mater. Chem.*, 2011, **21**, 2060-2063.
48. Z. Zapata-Benabithe, F. Carrasco-Marín and C. Moreno-Castilla, *J. Power Sources*, 2012, **219**, 80-88.
49. M.-C. Liu, L.-B. Kong, C. Lu, X.-M. Li, Y.-C. Luo and L. Kang, *RSC Adv.*, 2012, **2**, 1890-1896.
50. B. Xu, Y. Chen, G. Wei, G. Cao, H. Zhang and Y. Yang, *Materials Chemistry and Physics*, 2010, **124**, 504-509.
51. J. Wang, M. Chen, C. Wang, J. Wang and J. Zheng, *J. Power Sources*, 2011, **196**, 550-558.
52. K. Xia, Q. Gao, J. Jiang and J. Hu, *Carbon*, 2008, **46**, 1718-1726.
53. M. M. Bruno, N. G. Cotella, M. C. Miras, T. Koch, S. Seidler and C. Barbero, *Colloids Surf., A*, 2010, **358**, 13-20.
54. X. Yu, J.-g. Wang, Z.-H. Huang, W. Shen and F. Kang, *Electrochemistry Communications*, 2013, **36**, 66-70.
55. Z. Zapata-Benabithe, F. Carrasco-Marín, J. de Vicente and C. Moreno-Castilla, *Langmuir*, 2013, **29**, 6166-6173.
56. M. Sevilla, S. Álvarez, T. A. Centeno, A. B. Fuertes and F. Stoeckli, *Electrochim. Acta*, 2007, **52**, 3207-3215.

Table 1. Textural properties and chemical composition of carbon samples

Sample	Textural properties			Chemical composition [wt %]			(N/C) Atomic ratio
	S_{BET} [m^2 g^{-1}]	V_p [cm^3 g^{-1}] [a]	V_{micro} [cm^3 g^{-1}] [b]	N	C	O	
CN-500-4	< 3	-	-	47.8	37.4	12.7	1.1
CN-650-4	< 5	-	-	31.3	51.9	14.9	0.52
CN-800-4	660	0.29	0.27	22.9	60.0	15.0	0.33
CN-850-4	880	0.37	0.36	13.1	72.8	12.8	0.15
CN-900-4	990	0.42	0.40	6.3	79.2	13.8	0.07
CN-650-2	< 5	-	-	31.9	56.2	10.2	0.49
CN-800-2	730	0.32	0.28	17.3	68.6	12.6	0.22
CN-850-2	950	0.41	0.38	13.1	77.6	8.5	0.14
CN-900-2	1040	0.42	0.41	5.9	81.8	11.6	0.06

prepared by the carbonization of potassium gluconate/melamine mixtures.

[a] Pore volume at p/p_o ~ 0.95; [b] Micropore volume determined by the t-plot technique.

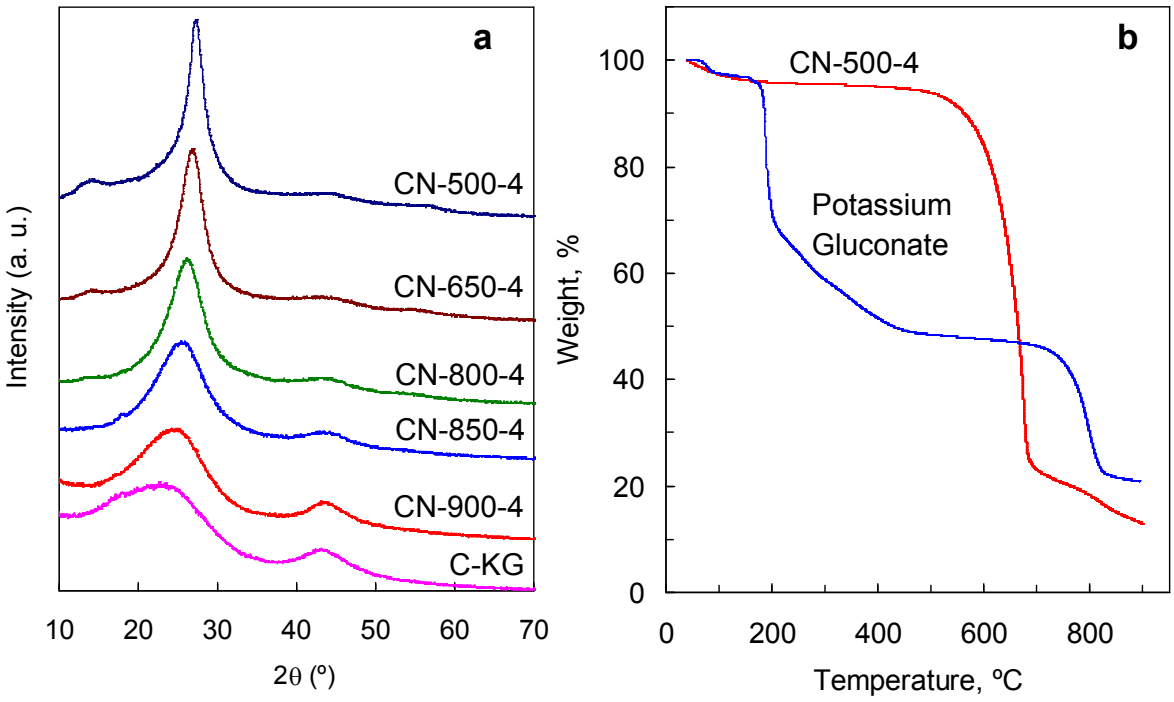

Figure 1. a) XRD patterns of carbon samples prepared by the carbonization of potassium gluconate (C-KG) and co-carbonization of potassium gluconate/melamine mixtures and b) TGA curves of potassium gluconate and CN-500-4 sample under a nitrogen flow (Heating rate: 3 ºC·min^{-1}).

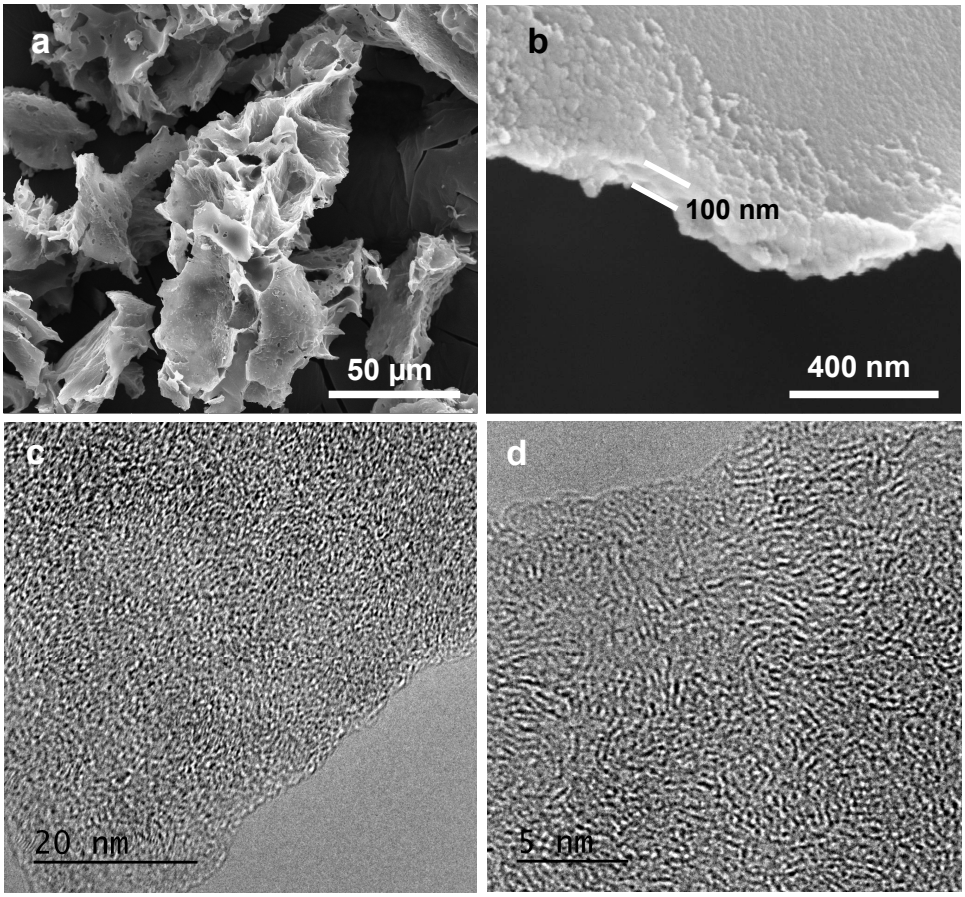

Figure 2. SEM (a, b) and TEM (c, d) images of the CN-800-4 sample.

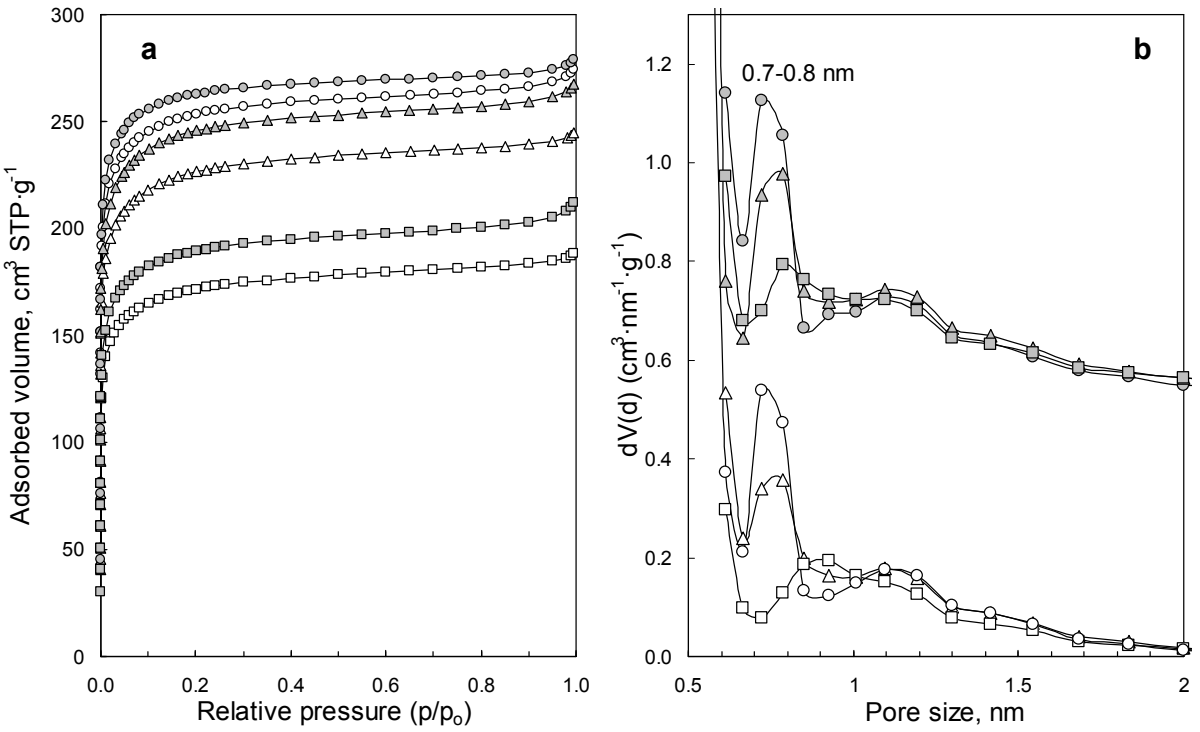

Figure 3. a) Nitrogen sorption isotherms and b) micropore size distribution (QSDFT method) for the carbon samples obtained by carbonization of melamine/potassium gluconate mixtures at 800 ºC (square symbols), 850 ºC (triangle symbols) and 900 ºC (circle symbols). Melamine/Gluconate weight ratios= 4 (white symbols) or 2 (grey symbols). The grey points in b) have been up-shifted by 0.55 $cm^3 \cdot nm^{-1} \cdot g^{-1}$ for clarity.

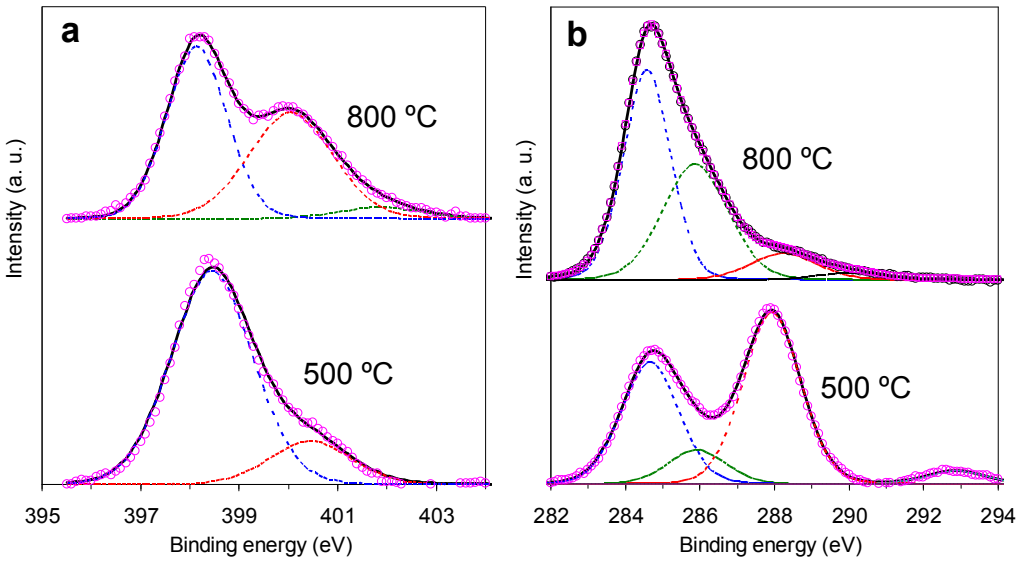

Figure 4. a) N 1s and b) C 1s XPS spectra of the samples synthesised at 500 ºC and 800 ºC [(melamine/potassium gluconate) weight ratio=4].

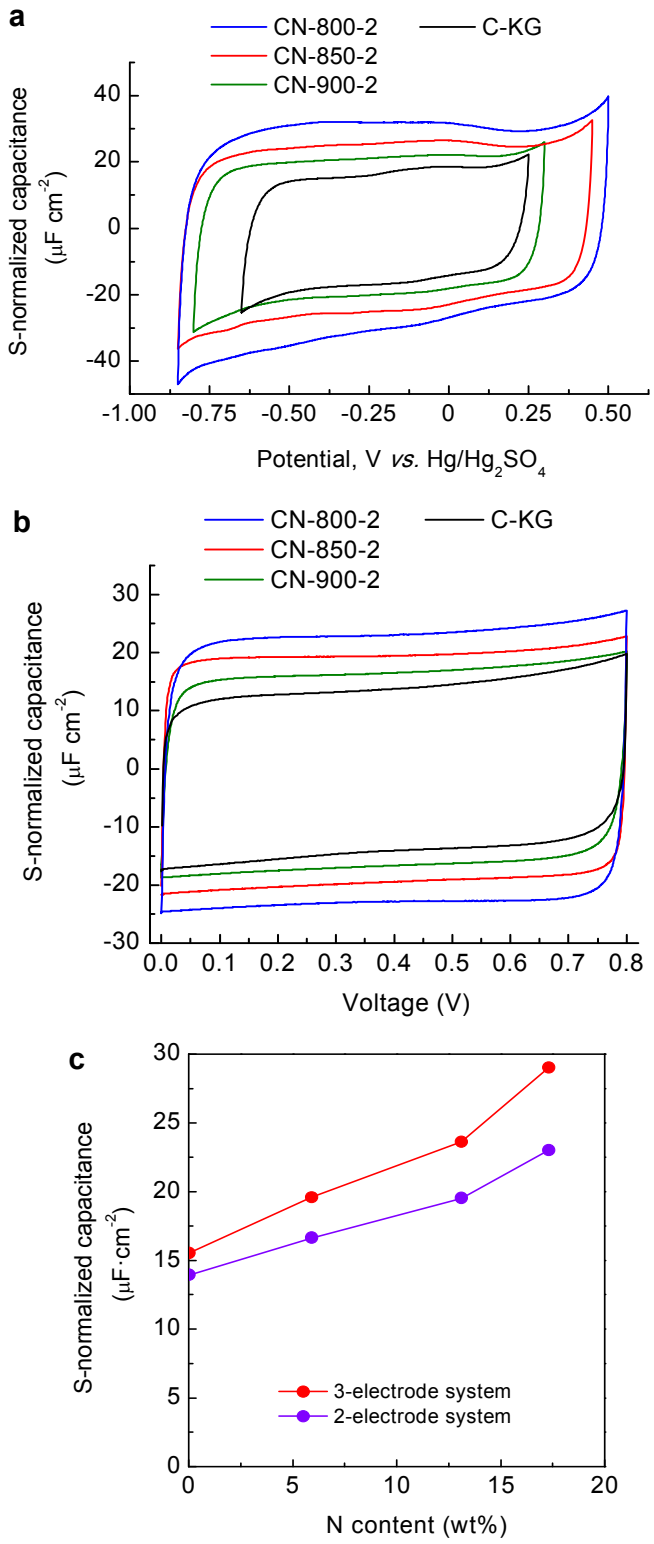

Figure 5. Cyclic voltammetry experiments (scan rate of 2 $mV \cdot s^{-1}$) in 1M H_2SO_4 electrolyte of the N-carbons and the undoped C-KG, using a three-electrode cell (a) and a two-electrode cell (b). (c) Variation of S-normalized capacitance with the nitrogen content.

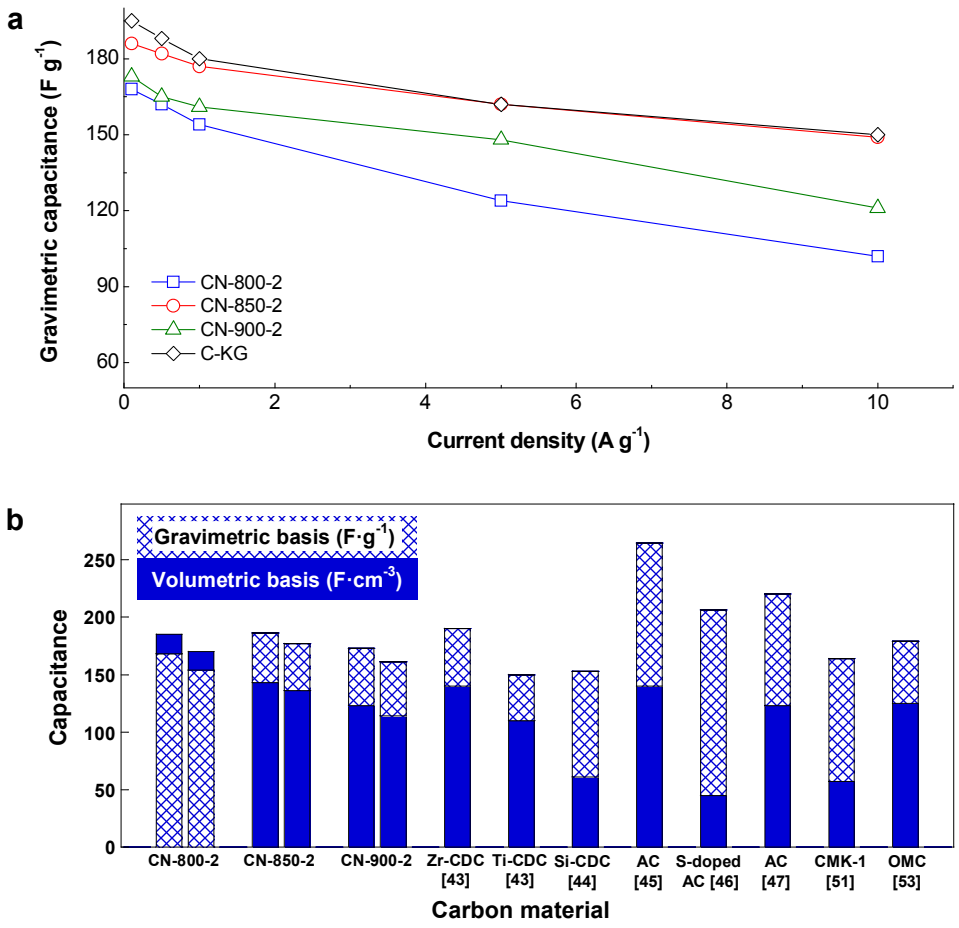

Figure 6. a) Evolution of specific capacitance with the increase in discharge current density in 1 M H_2SO_4 (2-electrode cell), b) comparison of the gravimetric and volumetric capacitance values at 0.1 A·g^{-1} and 1 A·g^{-1} of the N-carbons with those of CDCs, activated carbons and mesoporous carbons reported in the literature at low scan rates (2-5 mV·s^{-1})/low discharge current (0.1 A·g^{-1} or 1 mA·cm^{-2}). The values in the present work and those of references [43-45, 51] were measured in a two-electrode system, whereas those of references [46, 47, 53] correspond to a three-electrode system.

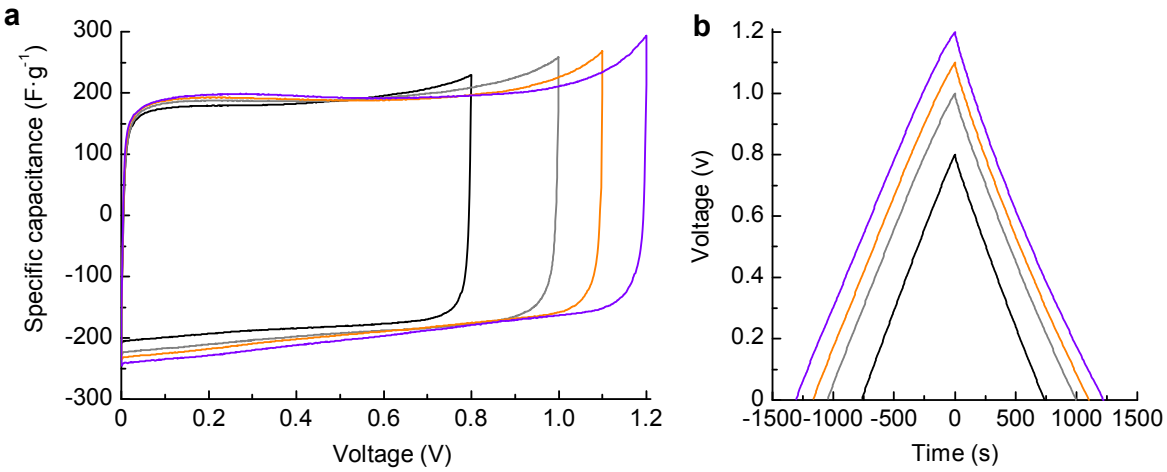

Figure 7. Enlargement of the cell voltage of the CN-850-2-based supercapacitor, analyzed by a) cyclic voltammetry at 2 $mV \cdot s^{-1}$ and b) galvanostatic charge/discharge at 0.1 $A \cdot g^{-1}$.

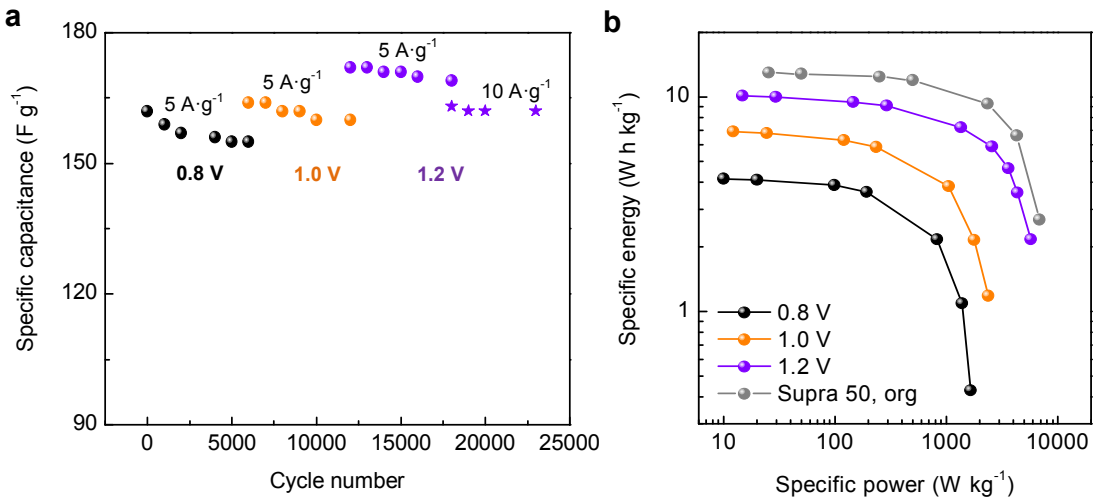

Figure 8. a) Long-term stability at different discharge current densities and b) Ragone plot of the CN-850-2-based supercapacitor for different maximum cell voltages in 1 M H_2SO_4. For comparison purposes, the Ragone plot of Supra 50 in 1 M $TEABF_4$/AN (2 V, active mass loading: 6 mg·cm^{-2}, pellets of 1 cm of diameter) has been included in (b).